The Impact of Wettability Alteration on Two-Phase Flow Characteristics of Sandstones - A Quasi-Static Description

Ahmed Al-Futaisi

Department of Civil and Environmental Engineering, University of California at Berkeley, CA, USA,
Department of Civil Engineering, Sultan Qaboos University, Al-Khoudh, Oman

Tad W. Patzek

Department of Civil and Environmental Engineering, University of California at Berkeley, CA, USA

Abstract. We describe a two-phase pore network simulator of drainage and imbibition, which integrates a realistic representation of pore connectivity and morphology, a quasi-static description of fluid displacement mechanisms, and a sound representation of the wetting properties of a sedimentary rock and of their alteration. The simulator works with 3D disordered networks of cylindrical ducts with triangular, square and circular cross-sections obtained directly from the analysis of micro-CT images of rock samples. All pore-level displacement mechanisms: piston-type, snap-off, and cooperative pore body filling are considered with arbitrary receding and advancing contact angles. Bond invasion percolation description is used in primary drainage, while bond-site invasion percolation with ordinary percolation on a dual network and compact cluster growth are used in secondary imbibition. In the paper, we resolve how to calculate the relative permeability of NAPL in the quasi-static approximation of imbibition, and illustrate spatial distribution of the clusters of trapped NAPL using our generalization to disordered networks of the Hoshen-Kopelman cluster-labelling algorithm. To understand the impact of wettability alteration on the capillary pressure and relative permeability functions, we perform a series of drainage and imbibition simulations by changing the range of advancing contact angles. Our study indicates that in imbibition, transport properties of a permeable solid are quite sensitive to the hysteresis between the receding and advancing contact angle. This sensitivity reflects competition among the different displacement mechanisms, which shapes the relative permeabilities, capillary pressures, and the distribution of the trapped NAPL.

1. Introduction

Transport of immiscible fluids, non-aqueous phase liquids (NAPLs) and gases that co-exist with water in soils and rocks, is of fundamental interest to subsurface water management. Any prediction of temporal and spatial distributions of these fluids is sensitive to the macroscopic descriptors of the permeable solid (its absolute permeability) and the multiple fluids (their relative permeabilities and capillary pressure). These macroscopic descriptors are the volume-averaged continuum functions with origin in the displacement mechanisms at pore scale [*Bear*, 1972]. Therefore, the macroscopic transport of immiscible fluids can be predicted if there is an adequate description of the essential geometry and topology of the pore space, and a sufficient representation of the multiphase flow physics. Nowadays, pore network models have these qualities and have become indispensable in the investigations of multiphase flows in porous media encountered in petroleum and environmental applications.

Since the pioneering work of *Fatt* [1956a, b, c], pore network models with disparate representations of the pore space have been employed in the studies of multiphase flow. Examples of these models include (i) regular lattices of cylindrical ducts with cross-sections that are circles [*Dixit et al.*, 1999], stars [*Man and Jing*, 2000], squares [*Fenwick and Blunt*, 1998; *Blunt*, 1998; *Dillard and Blunt*, 2000], triangles [*Hui and Blunt*, 2000], or polygons [*Tuller et al.*, 1999]; (ii) lattices of converging/diverging cones [*Reeves and Celia*, 1996], and spatially-correlated pores [*Lowery and Miller*, 1995; *Knackstedt et al.*, 2001]; and (iii) disordered networks with variable coordination numbers [*Blunt and King*, 1991; *Lowery and Miller*, 1995]. The various pore network models have been reviewed in, e.g., [*Sahimi*, 1993; *Blunt*, 2001]. Most models are generated stochastically and usually do not represent natural permeable media. In contrast, advanced imaging techniques, such as micro-focused computed tomography (micro-CT) [*Coles et al.*, 1994; *Hazlett*, 1995] and serial sectioning [*Holt et al.*, 1996; *Lin and Cohen*, 1982], capture wealth of information about the microstructure of real sediments. The recent advancements in rock imaging have resulted in a quantitative jump in the pore network model capabilities [*Øren et al.*, 1998; *Patzek*, 2001].

Pore-network modelling is a three-step procedure. In the first step, thin sections, CT images and depositional models are used to extract a pore space model from a sample of sedimentary rock. In the second step, this pore space model is simplified by replacing the actual (e.g., imaged) pore shapes with the well-defined geometrical shapes such as ducts of circular, triangular or square cross-section. The output of this step is a pore-network representation of the sediment. Finally, in step three, the simplified pore network is used to simulate a multiphase displacement process, and to obtain the respective macroscopic relative permeability and capillary pressure functions. Therefore, the pore-scale models differ from the large-scale models in that the macroscopic constitutive relationships are

Paper number .
0043-1397 /02/$9.00

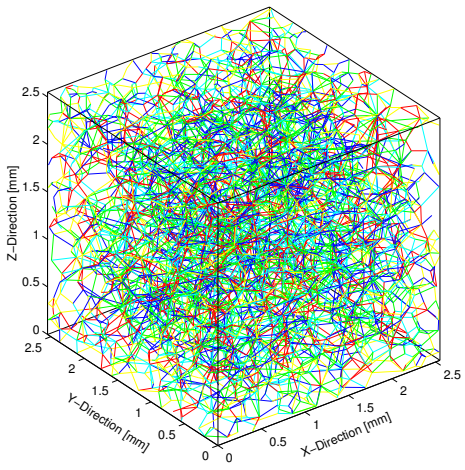

Figure 1. 3D network representation of pore throats (links or bonds) in Bentheimer sandstone

not assumed, but emerge from averaging of the relevant pore-scale physics. Using this three-step procedure, *Øren et al.* [1998] simulated two-phase flow in a sandstone and were able to *predict* the experimental drainage and imbibition capillary pressure and relative permeability curves.

The macroscopic transport properties of two-phase flow are determined not only by the geometry and topology of the porous medium, but also by the spatial distribution of wettability and the extent of wettability alteration in individual pores. Wettability may vary spatially owing to contaminant aging [*Powers et al.*, 1996], variation in aqueous chemistry [*Demond et al.*, 1994; *Powers and Tamblin*, 1995], mineralogy [*Anderson*, 1986], organic matter distributions [*Dekker and Ritsema*, 1994], and surface roughness [*Lenormand and Zarcone*, 1984; *Morrow*, 1975]. Several studies have used pore network models to investigate the effect of wettability on the macroscopic descriptors of two-phase flow [*Heiba et al.*, 1983; *McDougall and Sorbie*, 1995; *Blunt*, 1997a, b]. Common to all these models is the use of lattices to describe the sediment's pore space. In this paper we extend the analysis of wettability effects on the macroscopic capillary pressures, relative permeabilities, trapped NAPL distributions, and flow regimes using a faithful representation of the pore space of a permeable rock.

The paper is organized as follows. First, we briefly describe the disordered three-dimensional pore network used in this study. Second, we describe the physics of two-phase quasi-static drainage and imbibition of a single pore. Third, we describe the trapped NAPL clusters and provide procedures for identifying them in the network. Fourth, we calculate the network volume-averaged absolute permeability, the relative permeability and capillary pressure curves, the residual NAPL saturation, and the spatial distribution of clusters of the trapped NAPL. Full description of the percolation algorithms is provided. Finally, we study the effects of wettability on the network-averaged relative permeabilities and capillary pressure.

2. Network Generation and Description

The network, Figure 1, used earlier by Statoil [*Øren et al.*, 1998] and *Patzek* [2001], was extracted from a 3D micro-focused X-ray CT image of a $(2.5\text{mm})^3$ sample of Bentheimer sandstone. It consists of 3677 nodes (pore bodies or sites) and 8952 links (pore throats or bonds). All nodes and links are translationally-symmetric cylindrical ducts with arbitrary cross-sections (squares, triangles or circles). The network connectivity varies from zero to sixteen links connected to a node. The duct geometry is determined through two parameters: the inscribed circle radius, r, and the shape factor, G. The shape factor is defined as the ratio of the duct cross-sectional area and the square of its perimeter. The complex and variable cross sections of real pores are approximated with ducts of arbitrary triangular, square or circular cross-sections, such that the constant shape factors of the duct cross-sections are the axial averages of those calculated from the CT image. The most common cross-section of the network ducts is triangular. Given the shape factor, G, of an angular node or link, the corner half-angles, β_i, are generated using the procedure described in [*Patzek and Silin*, 2001]. The angular cylindrical ducts capture the most essential aspect of geometry of real pores: the presence of sharp corners filled with water that remains continuous across the network. We feel that the duct corners are more important than the converging-diverging geometry of circular ducts.

3. Pore-Level Descriptors of Two-Phase Flow

Figure 2 shows two immiscible fluids, water and NAPL, in contact with a smooth solid. The fluid configuration depends on how well each of the fluids wets the solid. This wetting ability is measured by the contact angle, θ, measured through the water. The diagram also depicts two different displacement regimes: drainage and imbibition. In drainage NAPL displaces water, whereas in imbibition water displaces NAPL. In general, these two displacement regimes result in different contact angles: receding contact angle, θ_r, in drainage and advancing contact angle, θ_a, in imbibition. Experiments have shown that advancing contact angle can be much larger than receding contact angle [*Morrow*, 1975; *Ma et al.*, 1996]. Drainage and imbibition can be repeated through multiple displacement cycles; however, we restrict this study to primary drainage where NAPL displaces water from a previously water-filled sediment (e.g., NAPL migration into groundwater) and secondary imbibition where water displaces the NAPL that invaded during primary drainage (e.g., NAPL clean-up by water flooding). Hysteresis between the receding and advancing contact angle contributes to the respective hystereses of the capillary pressure and the relative permeability curves; pore level displacement mechanisms contribute the rest.

Our goal is to calculate the capillary pressures and relative permeabilities in two-phase primary drainage and secondary imbibition of the network in Figure 1 with different arbitrary values of contact angles. Micromodel studies [*Lenormand et al.*, 1983; *Lenormand and Zarcone*, 1984; *Li and Wardlaw*, 1986] unveiled much of the pore-scale physics in two phase flow.

3.1. Displacement Mechanisms and Capillary Entry Pressure

There are two basic models of multiphase flow in pore networks: dynamic and quasi-static. In dynamic models, capillary, gravity, and viscous forces in the fluids are accounted for simultaneously. In quasi-static models, capillary forces dominate, gravity

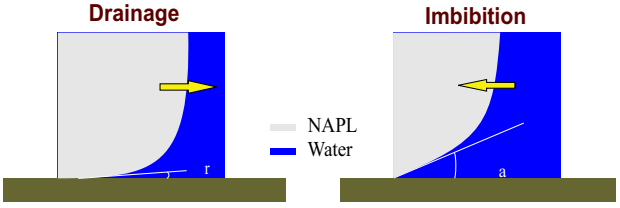

Figure 2. Contact angle hysteresis between drainage and imbibition

modifies the magnitude of capillary pressure, and the microscopic fluid distributions are frozen at each level of the capillary pressure. The hydraulic conductances of the resulting flow networks are then calculated independently. In this study we adopt the quasi-static approach and ignore the effects of viscous forces. We also ignore the effects of buoyancy forces[1].

When a node or link carries two fluids simultaneously, NAPL occupies the center of the pore and is treated as a bulk fluid, whilst water flows in the filaments along the pore corners, Figure 3. At the fluid interfaces, capillary pressure is given by the Young-Laplace equation:

$$P_c = P_N - P_w = \sigma\left(\frac{1}{r_1} + \frac{1}{r_2}\right) \tag{1}$$

where N and w label the NAPL and water, respectively; σ is the interfacial tension; and r_1 and r_2 are the principle radii of curvature of the fluid interface. Invasion by either of the fluids does not occur until this capillary pressure exceeds a specific threshold capillary entry pressure, P_c^e, that is different for the different displacement mechanisms and pore geometries. Primary drainage and secondary imbibition processes exhibit different pore-level invasion mechanisms. In primary drainage, the only invasion mechanism is piston-type displacement since initially the network is filled with water. In secondary imbibition, part of the network has been invaded by NAPL, and the displacement mechanisms include piston-type, snap-off and cooperative pore-body filling. This classification of pore level events was first presented in *Lenormand et al.* [1983]; *Lenormand* [1986], and the calculation of the corresponding capillary entry pressures is presented in, e.g., *Øren et al.* [1998]; *Patzek* [2001]. The pore-level displacement mechanisms are pivotal to the discussion of the effects of wettability. Therefore, we will briefly discuss them and provide more compact expressions of the capillary entry pressures.

First, let us define three constants that are common in most of the expressions for the capillary entry pressures. These constants are calculated for each corner, i, of an angular duct described by two parameters: the corner half-angle β_i, and contact angle, θ_i. The contact angle, θ_i, varies from the receding contact angle, θ_r, in primary drainage to the hinging or advancing contact angle, θ_h or θ_a, in secondary imbibition. The constants are

$$E_0^i = \frac{\pi}{2} - \theta_i - \beta_i \tag{2}$$

$$E_1^i = \frac{\cos(\theta_i + \beta_i)}{\sin(\beta_i)} \tag{3}$$

$$E_2^i = \frac{\cos(\theta_i + \beta_i)}{\sin(\beta_i)}\cos(\theta_i) \tag{4}$$

Constant E_0^i is positive in the case of primary drainage and spontaneous imbibition (concave menisci) and negative in the case of forced imbibition (convex menisci). The three constants are equal to zero for the ducts with circular cross-sections.

3.1.1. Drainage Piston-Type. By equating the radius of curvature of the arc-menisci (AM) in the corners to the first curvature of the invading interface [*Mayer and Stowe*, 1965], the threshold capillary entry-pressure can be expressed as

$$P^e_{c,PD}(\theta_r) = \frac{\sigma}{r}\cos(\theta_r)\left(1 + \sqrt{1 - \frac{4G\sum_{i=1}^{n}(E_2^i - E_0^i)}{\cos^2(\theta_r)}}\right) \tag{5}$$

where, E_0^i and E_2^i are calculated with $\theta_i = \theta_r$, and n is the number of corners in an angular duct, i.e., n =3 for triangles and n=4 for squares.

3.1.2. Imbibition Piston-Type. If there is contact angle hysteresis, each AM hinges about its contact line, pinned at a distance b_i from the corner apex, until the hinging contact angle, $\theta_{h,i}$, reaches advancing contact angle, θ_a. For a given capillary pressure P_c, the AM $\theta_{h,i}$ and the corresponding b_i are

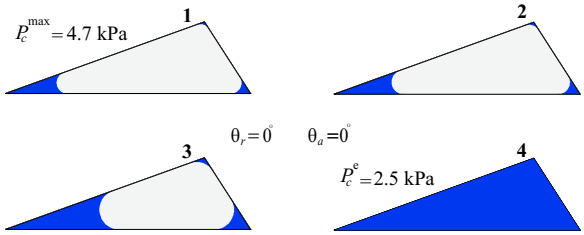

Figure 3. Distribution of water and NAPL in a single duct. In drainage a water-filled duct (4) is invaded by NAPL (3), and capillary pressure is further increased (2) and (1). Imbibition proceeds in the opposite direction

$$\theta_{h,i}(P_c) = \arccos\left[\frac{P_c}{P_c^{max}}\cos(\theta_r + \beta_i)\right] - \beta_i \tag{6}$$

$$b_i(P_c, \theta_{h,i}) = \frac{\sigma}{P_c}E_1^i \tag{7}$$

where P_c^{max} is the maximum capillary pressure in primary drainage.

Piston-type displacement in secondary imbibition can be spontaneous or forced. Spontaneous piston-type imbibition occurs at a positive capillary pressure, whereas forced imbibition occurs at a negative capillary pressure. The maximum advancing contact angle at which spontaneous secondary imbibition can occur is

$$\theta_{a,max} \approx \arccos\left(\frac{-4G\sum_{i=1}^{n}\cos(\theta_r + \beta_i)}{\left(\frac{rP_c^{max}}{\sigma}\right) - \cos(\theta_r) + 4nG\sin(\theta_r)}\right) \tag{8}$$

The threshold capillary pressure in spontaneous imbibition can be calculated by solving iteratively the following two equations:

$$\theta_i = \min\left\{\theta_{h,i}\left(\frac{\sigma}{r_{PT}}\right),\ \theta_a\right\} \tag{9}$$

$$r_{PT} = \frac{\frac{r^2}{4G} + r_{PT}^2\sum_{i=1}^{n}(E_0^i - E_2^i)}{2r_{PT}\sum_{i=1}^{n}E_0^i + \left(\frac{r}{2G} - 2r_{PT}\sum_{i=1}^{n}E_1^i\right)\cos(\theta_a)} \tag{10}$$

Eq. 9 calculates the actual contact angle, which will be the smaller of the hinging and advancing contact angle. This contact angle is used to calculate the constants E_0^i, E_1^i and E_2^i, which in turn are used to calculate the radius of curvature, r_{PT}, at the capillary entry pressure in Eq. 10.

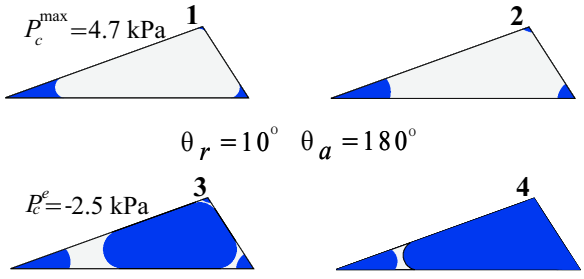

Figure 4. Creation of intermediate layers ($1 \rightarrow 4$) of NAPL in piston-type imbibition with extreme contact angle hysteresis

Then, the threshold capillary pressure in piston-type imbibition reduces to three cases:

$$P^e_{c,PT} = \begin{cases} \frac{\sigma}{r_{PT}} & \text{if } \theta_{\rm a} \le \theta_{\rm a,max} \\ \frac{2\sigma\cos(\theta_a)}{r} & \text{if } \theta_{\rm a,max} < \theta_{\rm a} < \frac{\pi}{2} + \min(\beta_{\rm i}) \\ -P^e_{c,PD}\,(\pi - \theta_a) & \text{if } \theta_{\rm a} \ge \frac{\pi}{2} + \min(\beta_{\rm i}) \end{cases} \tag{11}$$

In the first case, the invading water interface spontaneously imbibes into the pore at a positive capillary pressure. In the second and third case, the invading interface is forced into the pore at a negative capillary pressure. What distinguishes the third case from the second one is the creation of intermediate NAPL layers shown in Figure 4; the constants E^i_0 and E^i_2 are calculated with $\theta_i = \pi - \theta_a$. A NAPL layer in a corner is assumed to exist as long as the two confining menisci do not touch. The mathematical formulation of this condition is given in *Al-Futaisi and Patzek* [2002b] as function of the two interface-apex distances, the contact angles and the corner half-angle.

3.1.3. Snap-Off. Snap-off is the expulsion of NAPL by the swelling corner filaments, or AMs, of water[2]. Snap-off occurs if two or more of the AMs meet and fuse at a threshold capillary pressure. At this critical pressure, the AMs become unstable and the entire pore fills with water. Snap-off can only occur if there is no invading water interface waiting at an end of the pore (i.e., if piston-type is impossible). If the threshold capillary entry-pressure is positive, snap-off is spontaneous, whereas if it is negative, snap-off is forced. The maximum advancing contact angle at which spontaneous snap-off can occur is

$$\theta_{a,max} = \frac{\pi}{2} - \min(\beta_i) \tag{12}$$

In order to calculate the snap-off threshold capillary entry-pressure for triangular pores, one should first determine the radii of curvature of the menisci, $r_{so_{ij}}$, resulting from the meeting of the AM in the corner, i, with that in the adjacent corner, j:

$$r_{so_{ij}} = r\frac{cot(\beta_i) + \cot(\beta_j)}{E^i_1 + E^j_1} \tag{13}$$

Here the constants, E^i_1 and E^j_1, are determined using the minimum of the hinging contact angle, $\theta_h(\sigma/r_{_{SO_{ij}}})$, and the advancing contact angle, θ_a, for corners i and j, respectively. Since θ_h is a function of $r_{_{SO_{ij}}}$, iteration is required. The threshold capillary entry-pressure for snap-off is given by

$$P^e_{c,so} = \begin{cases} \frac{\sigma}{\min(r_{so_{ij}})} & \text{if } \theta_{\rm a} < \theta_{\rm a,max} \\ P^{max}_c \frac{\cos(\theta_a + \min(\beta_i))}{\cos(\theta_r + \min(\beta_i))} & \text{if } \theta_{\rm a,max} < \theta_{\rm a} < \pi - \min(\beta_{\rm i}) \\ P^{max}_c \frac{-1}{\cos(\theta_r + \min(\beta_i))} & \text{if } \theta_{\rm a} \ge \pi - \min(\beta_{\rm i}) \end{cases} \tag{14}$$

In the last two cases, all three AMs are convex, their curvatures are negative and water invasion is forced. When one of the AMs becomes a half-circle, it becomes unstable and snap-off occurs. Note that for $\theta_a = \theta_{a,max}$, the threshold capillary entry-pressure for snap-off is zero (a flat meniscus in the sharpest corner advances). Also, note that pores and throats with circular cross-sections do not have snap-off since there are no corners.

3.1.4. Cooperative Node Filling. The threshold capillary pressure necessary to fill a node with water depends on the smallest radius of curvature of the interface between the water and NAPL, and on the number of connected links. The required radius of curvature depends on the size of the node, and the number and spatial distribution of the connected links filled with NAPL. *Blunt* [1997b] represented the threshold node filling capillary pressure for the I_k mechanism (k is the number of links filled with NAPL):

$$P^e_{c,I_k} = \frac{2\sigma}{R_k} \tag{15}$$

where R_k is the mean or effective radius of curvature for filling by an I_k mechanism. We assume that I_1-mechanism is the same as the piston-type in imbibition described in Section 3.1.2. For I_2-mechanism and above, we use a similar procedure for calculating R_k, presented in [*Patzek*, 2001].

3.2. Saturations, Conductances, and Nodal Pressures

Figures 3 and 4 show that water can fill the entire pore, the corners of the pore, and/or the center of the pore. NAPL, in contrast, occupies the center of the pore or exists as sandwiched layers near the pore corners. *Øren et al.* [1998]; *Patzek* [2001] provide expressions for calculating phases areas, volumes, and saturations of both fluids. The hydraulic conductances are calculated using the expressions in *Patzek and Silin* [2001]; *Patzek and Kristensen* [2001]. The sandwiched NAPL layer geometry, stability, and conductance are detailed in *Al-Futaisi and Patzek* [2002b]. For simplicity, we assume that the overall conductance is calculated as a harmonic mean of the conductances of a unit flow channel consisting of a link and its two nodes (see *Patzek* [2001]). Since the fluids are incompressible, volume conservation is applied, and a set of linear algebraic equations for the node pressures are determined iteratively with a conjugate gradient method preconditioned by an incomplete LU decomposition.

4. NAPL Clusters

In primary drainage, NAPL invading the strongly water-wet nodes and links forms a single cluster always connected to the inlet. After breakthrough, this NAPL flows through a part of the network and is also connected to the outlet. Water corner filaments always remain connected throughout the network.

In secondary imbibition, bypassing, snap-off and cooperative pore-body filling gradually break the single NAPL cluster into many disconnected clusters with different configurations. We depict four possible types of NAPL clusters: clusters connected to the inlet and outlet faces (Type I), clusters connected to the outlet face but disconnected from the inlet face (Type II), clusters disconnected from the inlet and outlet faces (Type III), and finally clusters disconnected from the outlet face but connected to the inlet face (Type IV).

Identification of these clusters is *the* major task in the simulation of secondary imbibition; it is needed in order to update the percolation algorithm and to study the spatial distribution of the trapped NAPL. Therefore, an efficient cluster identification algorithm is required. In the percolation algorithm, if we only invade the NAPL clusters that are connected to the outlet (Type I and Type II), it is sufficient to identify these clusters with a spanning-tree searching algorithm starting from the outlet. However, to study the spatial characteristics of the trapped NAPL clusters (Type III and Type IV), a more sophisticated algorithm is required. In this study, we have chosen the famous Hoshen-Kopelman (HK) algorithm [*Hoshen and Kopelman*, 1976] to identify the latter cluster types.

The introduction of the Hoshen-Kopelman (HK) algorithm was an important breakthrough in the analysis of cluster size statistics in percolation theory. Although the algorithm was initially applied in statistical physics, nowadays it is used in many diverse fields [*Zhang and Seaton*, 1996; *Moreira and Barrufetb*, 1996; *Eddi et al.*, 1996; *Kinney et al.*, 1994; *Hamimov et al.*, 1989]. The algorithm has

been used in *ordered* lattices with only links, only nodes, or both links and nodes [*Hoshen et al.*, 1979; *Campos et al.*, 1997; *Hoshen*, 1980]. The HK algorithm is well-developed for lattice environments, and less developed for non-lattice environments, such as the *disordered* networks considered here. In a separate paper [*Al-Futaisi and Patzek*, 2002a], we present an efficient extension of the HK algorithm to complex disordered networks, cf. Figure 1. This extension of the HK algorithm is used here to identify the trapped NAPL clusters.

5. Macroscopic Fluid Transport Properties

The macroscopic fluid transport properties are calculated on the entire pore network. They are: the absolute permeability, capillary pressure, and two relative permeabilities.

5.1. Absolute Permeability

First, we determine the single-phase flow permeability of the network [*Dullien*, 1992]. Darcy's law [*Darcy*, 1856] for linear flow of an incompressible fluid defines the absolute permeability, k, of a sediment as follows:

$$k = \frac{Q}{A}\frac{\mu L}{\Delta P}, \tag{16}$$

where Q is the total volumetric flow rate, A is the normal cross-sectional area of the sample of the porous medium, μ is the fluid viscosity, ΔP is the pressure drop across the sample, and L is the sample length. Absolute permeability is a macroscopic transport property that is uniquely determined by the pore structure. The following procedure is implemented to calculate the absolute permeability:

1. Fully saturate the entire network with a single fluid
2. Calculate hydraulic conductances of the network ducts
3. Apply volume conservation to each node
4. Impose pressures on the inlet and outlet boundaries
5. Calculate the nodal pressures
6. Calculate the total inflow or total outflow
7. Apply Darcy's law (Eq. 16) to calculate the absolute permeability

The network used in this analysis has an absolute permeability of 5100 mDarcy. The rock permeability obtained by Statoil was 5160 mDarcy. To check the applicability of Darcy's law in our analysis, the yz-averaged nodal pressure distribution along the network x-axis is plotted in Figure 5. The figure indicates that the fluid pressure decreases linearly from the inlet face to the outlet face except for the minor boundary effects close to the faces; the flow in the network follows Darcy's law.

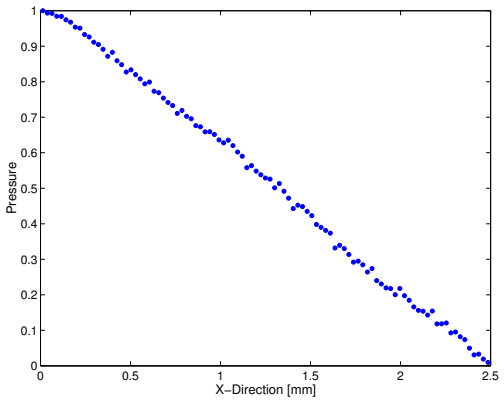

Figure 5. The cross-section averaged pressure distribution for fluid flow in the x-direction of the network in Figure 1

5.2. Capillary Pressure Curve

Drainage of an initially water-filled network proceeds by increasing capillary pressure level in the network. This is done in increments of link capillary entry pressures in piston-type displacement, ordered from lowest to highest. Drainage stops when a specified maximum capillary pressure is reached. Now imbibition begins and capillary pressure is lowered in steps of capillary entry pressures for all three displacement mechanisms ordered from highest to lowest. This ordering makes it plain that piston type displacement is most favored and snap-off is least favored. Imbibition stops when the last cluster of NAPL becomes disconnected from the outlet. At set capillary pressures (or overall water saturations), steady-state creeping flow of both phases is calculated on the cluster of water and those clusters of NAPL that are connected to the inlet and the outlet. Both phases are under a unit pressure difference.

In a permeable rock, fluid flow paths are determined by the rock, but the rock itself is in some sense random: fluid transport is a percolation process [*de Gennes*, 1980]. In two phase flow, the invading fluid must be connected to the inlet to continue invasion and the defending fluid must be connected to the outlet to be displaced. This dynamic percolation is called invasion percolation [*Wilkinson and Williamsen*, 1983]. If clusters of the defending fluid can be disconnected from the outlet, we call this process percolation with trapping [*Dias and Wilkinson*, 1986]. In primary drainage, the invading fluid is NAPL and it does not occupy the pore corners. Therefore, primary drainage is a pure *bond invasion-percolation* problem with a single piston-type displacement mechanism.

In contrast, imbibition is a problem in *mixed bond and site (link/node) invasion-percolation* and *ordinary percolation* with *trapping*. The invading water occupies the corners of the ducts. As capillary pressure decreases, link filling starts by snap-off, if initially there are no invading central menisci, and then by piston-type imbibition. Snap-off is an ordinary percolation process. Piston-type displacement is an invasion percolation process. At the same time, the nodes attached to one or more invaded links, but having two or more uninvaded links, are subject to cooperative node filling by I_k events. The I_k mechanisms generate compact clusters of water with no apparent connectivity to the inlet.

5.2.1. Algorithm of Bond Invasion-Percolation (Primary Drainage).

1. Calculate all piston-type capillary entry pressures of links and sort them in strictly ascending order.

2. At each capillary pressure level, find all links that have capillary entry pressure, Eq. 5, less than the current level of capillary pressure, have not yet been invaded, and have at least one of the two attached nodes filled with NAPL.

3. Invade these links and the attached nodes if applicable. A node is ready for invasion if it is occupied by water and its piston-type capillary entry pressure, Eq. 5, is less than the current level of capillary pressure.

4. New links may now become available to invasion because the attached nodes have been invaded.

5. Repeat steps 2-3 until no further nodes or links can be invaded.

6. Having invaded all possible links and nodes, calculate the overall (average) water-phase saturation in the network.

7. Proceed to the next capillary entry pressure level and repeat steps 2-6 until the specified maximum capillary entry pressure is reached.

5.2.2. Algorithm of Mixed Invasion-Percolation and Ordinary Percolation with Trapping (Secondary Imbibition).

1. Secondary imbibition starts after a maximum capillary pressure level in primary drainage has been reached.

2. Starting from the maximum capillary pressure level, invade links or nodes with water in order of the decreasing piston-type, and snap-off capillary entry pressures. All these pressures are sorted in a single list in strictly descending order.

3. To be displaced by the invading water, NAPL must be connected to the outlet of the network. After primary drainage, the NAPL formed one cluster spanning the entire network. In imbibition, snap-off and I_k events, gradually break the initial NAPL cluster into many disjoint clusters. Since only the clusters connected to the outlet (type I and II) must be identified, use a spanning-tree searching algorithm [*Cheriton and Tarjan*, 1976] starting from the outlet node. To flag a water- or NAPL-type duct during cluster identification, we assume that if the duct contains NAPL in the center or in *at least one* sandwiched layer, it is NAPL-type. Otherwise, the duct is water-type. The assumption that a single sandwiched NAPL layer per duct provides connectivity with the neighboring ducts may overstate the overall NAPL cluster connectivity. It is difficult to track the spatial orientation of the intermediate layers in a network because of the complex network geometry and topology, and lack of information about the orientation of its nodes and links.

4. Once the NAPL clusters connected to the outlet face are identified, the invasion process is restricted to the links and nodes in these clusters leaving the rest of the clusters trapped. In the case of links, first check the viability of piston-type displacement. A link undergoes a piston-type displacement if its piston-type capillary entry pressure, Eq. 11, is greater than the current capillary pressure level, and it has at least one of its two nodes filled with water. If neither of the nodes is filled with water, check for the possibility of snap-off if the link snap-off capillary entry pressure, Eq. 14, is greater than the current capillary pressure level. In the case of nodes connected to at least one link filled with water, and depending on the number of connected links that have NAPL, check the viability of cooperative node filling when the respective capillary entry pressure, Eq. 15, exceeds the current capillary pressure level. If the node is not connected to any link that has water phase, perform snap-off if the node snap-off capillary entry pressure is greater than the current level of capillary pressure. If new nodes or links have become available for invasion, repeat this procedure until no further invasion is possible.

5. Before proceeding to the next capillary pressure level, update the saturations.

6. Repeat procedure 3-5 at the next, lower capillary pressure level.

5.3. Relative Permeability Curves

We compute relative permeability of phase i, using Darcy's law:

$$k_{r,i} = \frac{Q_i \, \mu_i \, L}{k \, A \, \Delta P_i} \tag{17}$$

where Q_i is the volumetric total flow rate of phase i, μ_i is the phase i viscosity, and ΔP_i is the phase i pressure drop across the network.

At several overall water-phase saturations, 40 in this analysis, we solve for the nodal pressures and then calculate each relative permeability by using Eq. 17 for water and NAPL. Since water remains continuous throughout the network, the nodal pressure calculation is applied to all nodes except the ones connected to the inlet and outlet faces and the ones that are dead-end. The inlet face nodes are assigned an arbitrary pressure P_{in}, whereas outlet face nodes are assigned arbitrary pressure P_{out}. Dead-end pores do not flow, and are eliminated from the calculation.

The NAPL clusters can be of the four types depicted in Section 4. In the relative permeability calculations, it is reasonable to ignore all clusters disconnected from the outlet face (type III and IV) because these clusters are trapped and hence cannot be displaced by the invading water. However, it is essential to consider the remaining two cluster types that are connected to the outlet face because they can flow. These two cluster types have different boundary conditions and therefore the reasons for their inclusion in the calculations are different.

The clusters connected to the inlet and outlet faces (type I) span the entire network and their boundary pressures are simply P_{in} for the nodes on the inlet face and P_{out} for the nodes on the outlet face. Thus, the calculation of the NAPL permeability for these clusters follows a procedure similar to that implemented in drainage. Note that the conductances of water filaments are different, because each corner filament may have its own hinging angle. In contrast, the boundary condition for the nodal pressure calculation of type II clusters is P_{out} for the nodes on the outlet face, and the NAPL pressures on the internal boundary of the clusters. The internal boundary is defined as any NAPL node in the cluster that is connected to a link filled with water. Another important difference between these two cluster types is that the inflow and outflow in type I clusters are both NAPL, whereas in the case of type II clusters, the inflow is water and the outflow is NAPL.

To our knowledge, all quasi-static pore network simulators ignore the contributions of type II-IV clusters to the NAPL relative permeability. Only type I clusters that span the entire network are considered. This approach is consistent with the assumption that only steady-state relative permeabilities can be calculated by a quasi-static pore network simulator. Inclusion of type II clusters would be equivalent to the calculation of unsteady state relative permeability of NAPL, whereby water accumulates in the network and expels the type II clusters. Unsteady state calculations are impossible within the quasi-steady state framework, and type II clusters are ignored in the relative permeability calculations. Type II clusters are *not* ignored in the capillary pressure calculations. The lowest trapped NAPL saturation is achieved when the last type II cluster is expelled from the network.

6. Macroscopic Effects of Wettability Alteration

The receding contact angle during primary NAPL invasion is assumed to be zero because initially the sediment is fully saturated with water. As seen from Figure 3, after primary drainage the NAPL occupies the pore centers and the water resides in the corners. After invasion, the water films covering the central part of each of the pore walls may rupture and the walls may become NAPL-wet[3] [*Kovscek et al.*, 1993], whereas the pore corners remain water-wet resulting in a mixed-wet rock, first described by *Salathiel* [1973]. As a result, prior to secondary imbibition, wettability of the pore interior is altered (i.e., the small receding contact angle in drainage changes to a larger advancing contact angle in imbibition [*Buckley et al.*, 1995; *Buckley and Liu*, 1998; *Hirasaki*, 1991; *Morrow et al.*, 1986; *Freer et al.*, 2002]). The degree of wettability alteration is spatially variable and depends on the mineralogy of the surface and the chemical composition of the fluids [*Buckley et al.*, 1995; *Buckley and Liu*, 1998; *Hirasaki*, 1991; *Morrow et al.*, 1986]. In the following sections, we use the displacement scenario described above to study the effect of wettability alteration on the capillary pressure, trapped NAPL clusters, relative permeabilities, and displacement mechanisms. In our calculations, we have used 35 mN/m for the interfacial tension, 1 mPa-s for the fluid viscosities, 188 kPa for

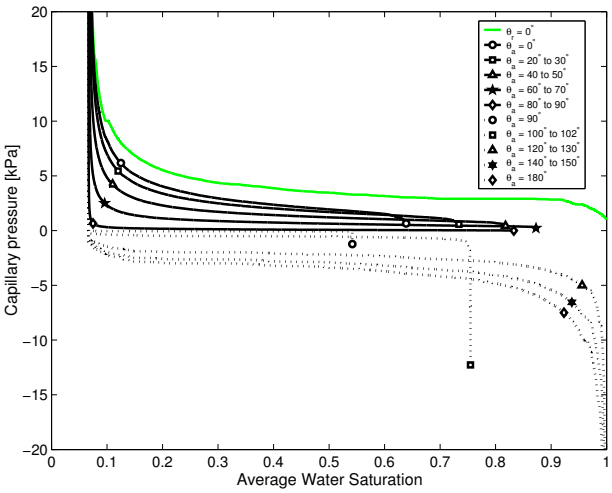

Figure 6. Impact of advancing contact angles on the secondary imbibition capillary pressure

the maximum P_c in primary drainage, and the no-slip boundary condition at the NAPL-water interfaces. The densities of the two fluids are the same.

6.1. Effects on Capillary Pressure Curve and Trapped NAPL

The advancing contact angles 0° to 180° are divided into several smaller ranges (see Figures 6 to 9). Within each range, the contact angles are spatially variable in the network, with uniform random distribution, reflecting the heterogeneous pore-surface chemistry and roughness. Figure 6 shows that the secondary imbibition capillary pressure curves change significantly in response to the range of advancing contact angles. As we increase contact angle hysteresis, we increase the capillary pressure hysteresis. With no contact angle hysteresis, $\theta_r = \theta_a = 0^\circ$, the capillary pressure hysteresis is caused by the different percolation mechanisms in primary drainage and secondary imbibition. For $\theta_a = 0^\circ$ to 90°, the capillary pressure is positive and imbibition spontaneous. The imbibition curves become flatter as we approach $\theta_a = 90^\circ$. As seen from Figure 6, the range $\theta_a = 80^\circ$ to 100° generates an almost completely flat curve close to $P_c = 0$ kPa. Further increase of advancing contact angles results in forced imbibition, in which capillary pressure becomes negative. In this case, the imbibition capillary pressure curves cease being flat. For $\theta_a \geq 120^\circ$, these curves mirror the primary drainage capillary pressure curve.

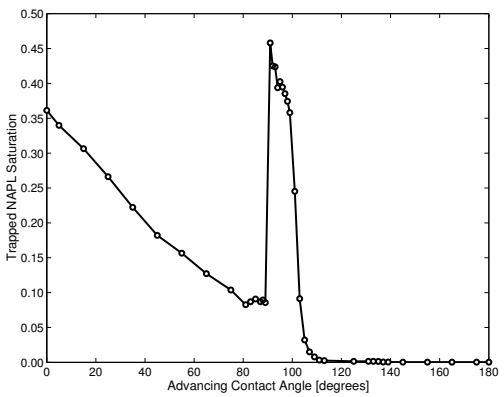

Figure 7. Trapped NAPL saturation as a function of advancing contact angles

Figure 6 also shows the dramatic effects of advancing contact angles on the trapped NAPL saturation. The relation between the trapped NAPL saturation and the advancing contact angle is summarized in Figure 7. In the case of water-wet network, the trapped NAPL saturation decreases as the advancing contact angles increase. The saturation reduction is from 38% for the strongly water-wet network, $\theta_a = 0^\circ$, to about 9% for the case of weakly water-wet network, θ_a just below 90°. The transition between water- and NAPL-wetness of pore centers, $\theta_a \approx 90^\circ$, results in a dramatic jump in the trapped NAPL saturation, from 8% to almost 46%. This jump should be expected because of the transition in the dominating displacement mechanisms between a water-wet and NAPL-wet network. As previously seen from Figure 4, the creation of intermediate NAPL layers is one of the important characteristics of flow in the NAPL-wet regime. These layers enhance the connectivity of NAPL in the network and thus reduce the NAPL trapping. However, for contact angles $\theta_a = 90^\circ$ to 100°, it is geometrically impossible to create any such layers, resulting in high NAPL trapping. For contact angles $\theta_a = 100^\circ$ to 120°, some stable NAPL layers are created and trapped NAPL saturation starts to decrease. Figure 7 clearly shows the high sensitivity of the trapped NAPL saturation to the advancing contact angles between 90° to 120°. This sensitivity reduces with the increasing number of intermediate NAPL layers. For contact angles larger than 120°, very low saturations of trapped NAPL can be reached. The trapped NAPL saturation for $\theta_a = 180^\circ$ is 0.03%. In Figure 8, the spatial distributions of the trapped NAPL clusters are plotted for four intervals of advancing contact angles. The clusters are identified using our modification of the Hoshen-Kopelman algorithm to disordered networks. The numbers of trapped NAPL clusters for $\theta_a = 10^\circ$ to 20°, 70° to 80°, 92 to 94°, and 170 to 180° are $618, 336, 2699, 571$, respectively. A detailed description of the statistical and fractal properties of these clusters will be addressed in a separate paper.

6.2. Wettability Effects on Relative Permeability Curves

Figure 9 shows how the relative permeabilities change in response to the increasing advancing contact angles. To find a pattern in these changes, we group the results into four wettability ranges: $\theta_a = 0^\circ$ to 45°, $\theta_a = 45^\circ$ to 90°, $\theta_a = 90^\circ$ to 120°, and $\theta_a = 120^\circ$ to 180°. For $\theta_a = 0^\circ$ to 45°, Figure 9a, the change in the relative permeability to water is minor. The relative permeability to NAPL is initially (for $S_w < 0.5$) the same; however, as the water saturation increases, considerable variation is observed. Larger advancing contact angles result in the higher NAPL relative permeabilities. In contrast, for $\theta_a = 45^\circ$ to 90° (Figure 9b), the NAPL relative permeabilities undergo small changes, but the water relative permeabilities change dramatically. Larger advancing contact angles result in smaller water relative permeabilities and a slight increase in the relative permeability to NAPL. In the range $\theta_a = 90^\circ$ to 100°, Figure 9c, the water relative permeability is very low because water moves almost entirely in the corner filaments. The NAPL relative permeability is also low due to significant trapping. As soon as θ_a departs from 100°, the water relative permeability increases and does not change further as we continue increasing advancing contact angles. In contrast, the relative permeability to NAPL first increases (9a), then stays constant (9b), jumps (9c), and finally levels off (9d).

Comparing Figures 9a- 9d, one concludes that the relative permeability to water undergoes a small variation across all wettability scenarios, except for $\theta_a = 45^\circ$ to 100°, where the variation is dramatic. On the other hand, the relative permeability to NAPL shows small variations for all wettability scenarios, except for the $\theta_a = 0^\circ$ to 45° and $\theta_a = 90^\circ$ to 120°, where large changes are apparent.

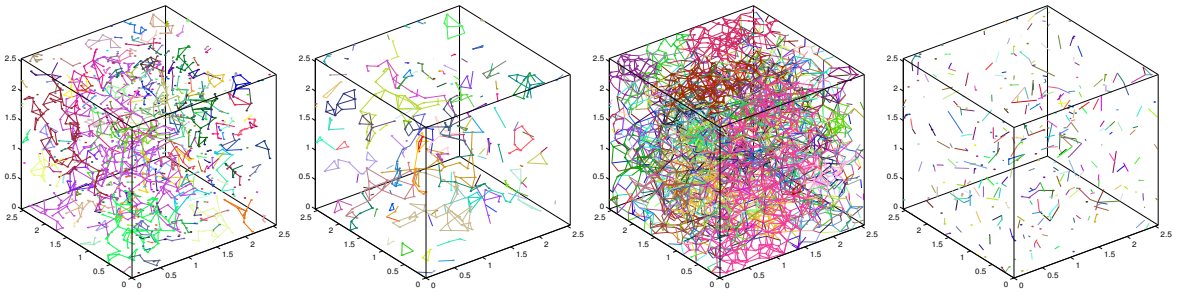

(a) $\theta_a = 10°$ to $20°$ (b) $\theta_a = 70°$ to $80°$ (c) $\theta_a = 92°$ to $94°$ (d) $\theta_a = 170°$ to $180°$

Figure 8. Spatial distributions of clusters of trapped NAPL for the indicated ranges of advancing contact angles

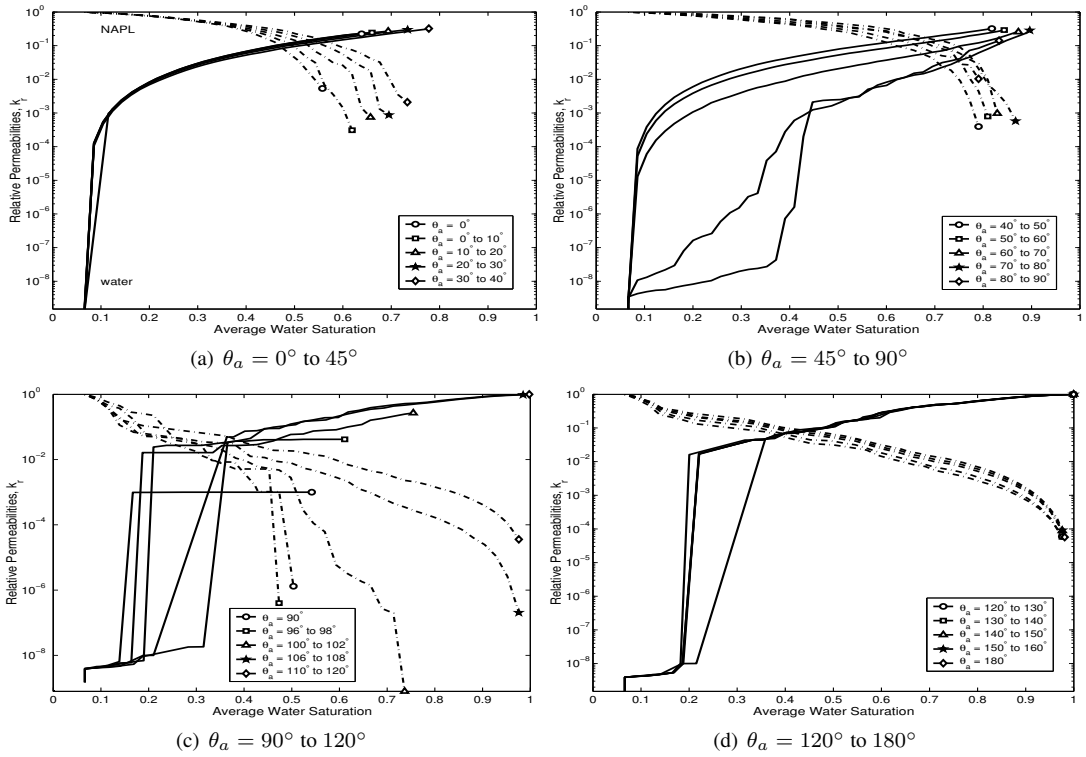

(a) $\theta_a = 0°$ to $45°$ (b) $\theta_a = 45°$ to $90°$

(c) $\theta_a = 90°$ to $120°$ (d) $\theta_a = 120°$ to $180°$

Figure 9. Impact of advancing contact angle on the secondary imbibition relative permeabilities in water-wet and NAPL-wet networks

One can also observe that for water saturations less than 50%, water flow is very slow (water relative permeability is less than 0.02). Similarly, for water saturations greater than 50%, NAPL flow is very slow (NAPL relative permeability is less than 0.02). Finally, one can observe that the crossover-points of water and NAPL relative permeabilities are roughly at saturations greater than 50% for the water-wet cases and less than 50% for the NAPL-wet cases.

6.3. Wettability Effects on Flow Regimes

The variability of two phase flow in porous media can be explained by the competition of the different pore-level displacement mechanisms in response to changes of advancing of contact angle, Figure 10. In strongly water-wet systems, $\theta_a = 0°$, link snap-off is favored. As capillary pressure decreases, snap-off fills the narrowest links with water throughout the network, and node filling is suppressed until most of the links are already filled. When most links are water-filled, the NAPL in the nodes is likely to be trapped. Therefore, the domination of snap-off mechanism is responsible for the largest trapped NAPL saturation observed in the strongly water-wet systems. As we increase contact angle hysteresis, snap-off is favored less and piston-type displacement starts to dominate. The invasion starts by snap-off in the smallest links throughout the network, i.e., by *ordinary percolation*, followed by piston-like cooperative node filling if the node/link aspect ratio is not too large, i.e., by *compact cluster growth* [*Lenormand et al.*, 1983]. The competition between different types of node filling mechanisms plays a major role in filling the nodes with water. The growth of compact water clusters leads to minor NAPL trapping, caused by bypassing or coalescence of the growing clusters of water-filled nodes and links. This observation indicates that in water-wet systems, the invasion of the water/NAPL central menisci present at the inlet face is favored less than snap-off in the network.

As the network (rock) becomes less water-wet and more NAPL-wet, i.e., $\theta_a + \beta > 90°$, a dramatic change in the flow regime occurs. The imbibition is forced, and therefore the cooperative node filling is completely suppressed. The competition is now between forced snap-off and forced piston-type displacement. However, for a piston-type displacement to occur, there must exist an invading interface somewhere in the network to initiate it. Therefore, if during primary drainage all pores were invaded by NAPL, and there are no water/NAPL central menisci waiting at the inlet face of the

network, snap-off must act first in order to start the invasion. It is seen in our simulation that forced snap-off rarely occurs, because it requires very large negative capillary pressures. Then, once one or more snap-off events occur, the rest of the water invasion occurs at the same level of capillary pressure. However, if the water/NAPL interfaces exist at the inlet face, as in our case, the invasion will always be forced piston-type and snap-off will rarely be observed. Since now NAPL is wetting and water is nonwetting, the displacement is *invasion percolation with trapping*. The water advances by filling the largest links and nodes, which results in bypassing of significant amount of the NAPL due to the pinning of the corner menisci and the difficulty of creating stable NAPL layers, $\theta_a = 90^\circ$ to 100°. This regime results in the maximum trapped NAPL saturation. As we further increase advancing contact angle, $\theta_a \geq 110^\circ$, we start creating stable intermediate NAPL layers near the pore corners that allow better connectivity of the NAPL and hence less trapping. Trapping occurs when the NAPL layers collapse. Although the NAPL trapping for $\theta_a \geq 120^\circ$ is the least, the relative permeability to NAPL is very low.

7. Conclusions

We have presented a quasi-static simulator of drainage and imbibition of two immiscible, incompressible fluids in a three-dimensional, disordered network extracted from a real rock. We have computed the absolute permeability, the relative permeabilities, the capillary pressure curves, and the saturation and spatial distribution of clusters of the trapped NAPL. Our model allows for flow of wetting fluid in the pore corners, different contact angles, and different types of displacement mechanisms: piston-type, snap-off, and cooperative pore-body filling. Primary drainage is performed using bond invasion percolation, whereas imbibition is performed using bond-site invasion percolation and ordinary percolation. The spatial distribution of trapped NAPL clusters is illustrated using a modified Hoshen-Kopelman algorithm for disordered networks. Different ranges of advancing contact angles have been used to study the hysteresis of relative permeability and capillary pressure curves. In general, wettability alteration has a profound effect on the type of imbibition displacement and hence on the two-phase flow characteristics.

In water-wet rocks, invasion will always begin from within the rock by snap-off, resulting in high trapped NAPL saturation. However, as the advancing contact angle increases (the rock becomes weakly water-wet), snap-off becomes less favored and piston-type displacement from the initial snap-off events starts to form growing compact clusters. Competition between the different types of pore body filling mechanisms plays a major role in the invasion that results in decreasing the trapped NAPL saturation. Water relative permeability remains about the same for contact angles less that 45°, but it decreases very fast as the contact angle is further increased (until 90°). As the advancing contact angle increases, NAPL relative permeability increases slowly. In contrast to water-wet rocks, secondary imbibition displacement in NAPL-wet rocks begins by forcing water into the rock. Snap-off and cooperative pore body filling are almost completely suppressed. For $\theta_a = 90^\circ$ to 100°, water injection is an invasion percolation process with significant bypassing of NAPL. However, as the advancing contact angle increases, stable intermediate NAPL layers are created, resulting in a very low trapped NAPL saturation. In general, water relative permeability in the NAPL-wet rocks changes little. The variation of the relative permeability to NAPL is considerable in the range $90 - 120^\circ$. As we increase the advancing contact angle, we increase the relative permeability to NAPL.

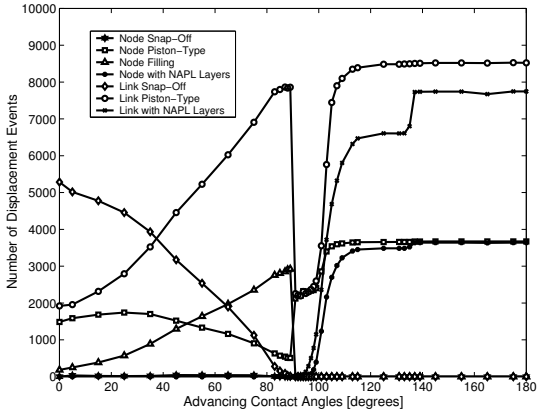

Figure 10. Effects of advancing contact angle on the secondary imbibition pore-level displacement mechanisms

Acknowledgements

We would like to thank the Reviewers for their thoughtful and very helpful comments and suggestions.

Notes

1. For very low capillary pressures, we are limited to look at fluids whose densities are similar.
2. Since we do not allow for the converging/diverging *angular* pore throats, there is no capillarity-driven water flow into the pore necks.
3. It now appears that presence of *any* hydrocarbon next to a solid changes the wetting properties of the solid surface.

References

Al-Futaisi, A., and T. W. Patzek, Extension of the Hoshen-Kopelman algorithm to a non-lattice environment, *Physica A*, *In print, PHYSA 7173*, 2002a.

Al-Futaisi, A., and T. W. Patzek, Three-phase hydraulic conductances in angular capillaries, *SPE 75193. Proceedings of the 13th SPE/DOE Symposium on Improved Oil Recovery, Tulsa, Oklahoma*, 2002b.

Anderson, W. G., Wettability litreture survey: Part 3. rock/oil/brine interactions and the effects of core handling on wettability, *J. Petrol. Technol.*, *38*, 1125–1144, 1986.

Bear, J., *Dynamics of Fluids in Porous Media*, Dover, Mineola, N. Y., 1972.

Blunt, M. J., Effects of heterogeneity and wetting on relative permeability using pore level modeling, *Soci. Petro. Engrg. J.*, *2*, 70–87, 1997a.

Blunt, M. J., Pore level modeling of the effects of wettability, *Soci. Petro. Engrg. J.*, *2*, 494–510, 1997b.

Blunt, M. J., Physically-based network modeling of multiphase flow in intermediate-wet porous media, *J. Petro. Sci. Engin.*, *20*, 117–125, 1998.

Blunt, M. J., Flow in porous media: Pore-network models and multiphase flow, *Curr. Opin. Colloid Interface Sci.*, *6*, 197, 2001.

Blunt, M. J., and P. King, Relative permeabilities from two- and three-dimensional pore-scale network modelling, *Trans. Porous Media*, *6*, 407–433, 1991.

Buckley, J. S., and Y. Liu, Some mechanisms of crude oil/brine/solid interactions, *J. Petro. Sci. Engin.*, *20*, 155–160, 1998.

Buckley, J. S., C. Bousseau, and Y. Liu, Wetting alteration by brine and crude oil: From contact angles to cores, *SPE 30765. Proceedings of the SPE Annual Conference and Exhibition, Dallas*, 1995.

Campos, P. R. A., L. F. C. Pessoa, and F. G. B. Moreira, Cluster-size statistics of site-bond-correlated percolation models, *Phys. Rev. B*, *56*, 40–42, 1997.

Cheriton, D., and R. E. Tarjan, Finding minimum spanning trees, *SIAM Journal on Computing*, *5*, 724–742, 1976.

Coles, M. E., P. Spanne, E. L. Muegge, and K. W. Jones, Computed microtomography of reservoir core samples, *Proceedings of the International SCA Meeting Stavanger*, 1994.

Darcy, H., Les fontaines publiques de la ville de Dijon, *Victor Dalmont, Paris*, 1856.

de Gennes, P. G., Percolation- A new unifying concept, *La Recherche*, *7*, 919–26, 1980.

Dekker, L. W., and C. J. Ritsema, How water moves in a water repellent sandy soil, 1, potential and actual water repellency, *Water Resour. Res.*, *30*, 2507–2519, 1994.

Demond, A. H., F. N. Desai, and K. F. Hayes, Effect of cationic surfactants on organic liquid-water capillary pressure-saturation relationships, *Water Resour. Res.*, *30*, 333–342, 1994.

Dias, M. M., and D. Wilkinson, Percolation with trapping, *J. Phys. A*, *19*, 3131–3146, 1986.

Dillard, L. A., and M. J. Blunt, Development of a pore network simulation model to study nonaqueous phase liquid dissolution, *Water Resour. Res.*, *36*, 439–545, 2000.

Dixit, A. B., S. R. McDougall, K. S. Sorbie, and J. S. Buckley, Pore-scale modeling of wettability effects and their influence on oil recovery, *SPE Reservoir Evaluation and Engineering*, *2*, 25–36, 1999.

Dullien, F. A. L., *Porous Media: Fluid Transport and Pore Structure*, 2nd ed., Academic Press, INC, 1992.

Eddi, F., J. Mariani, and G. Waysand, Transient synaptic redundancy in the developing cerebellum and isostatic random stacking of hard spheres, *Biol. Cybern.*, *74*, 139–146, 1996.

Fatt, I., The network model of porous media I. Capillary pressure characteristics, *Trans. AIME*, *207*, 144–159, 1956a.

Fatt, I., The network model of porous media II. Dynamic properties of a single size tube network, *Trans. AIME*, *207*, 160–163, 1956b.

Fatt, I., The network model of porous media III. Dynamic properties of networks with tube radius distribution, *Trans. AIME*, *207*, 164–181, 1956c.

Fenwick, D. H., and M. J. Blunt, Three-dimensional modeling of three-phase imbibition and drainage, *Adv. Water Resour.*, *21*, 121–143, 1998.

Freer, E. M., T. F. Svitova, and C. J. Radke, Aging of the crude oil/brine interface: Implications for mixed wettability, *SPE 75188. Proceedings of the 13th SPE/DOE Symposium on Improved Oil Recovery, Tulsa, Oklahoma*, 2002.

Hamimov, S., M. A. Michalev, A. Savchenko, and O. I. Yordanov, Classification of radar signatures by autoregressive model-fitting and cluster-analysis, *IEEE Trans. on Geosci. Remote Sens.*, *27*, 606–610, 1989.

Hazlett, R. D., Simulation of capillary-dominated displacements in microtomographic images of reservoir rocks, *Trans. Porous Media*, *20*, 21–35, 1995.

Heiba, A. A., H. T. Davis, and L. E. Scriven, Effect of wettability on two-phase relative permeabilities and capillary pressures, *SPE 12127. Proceedings of the SPE Annual Conference, San Francisco*, 1983.

Hirasaki, G. J. S., Wettability: Fundamentals and surface forces, *SPE Form. Eval.*, *6*, 217–226, 1991.

Holt, R. M., E. Fjaer, O. Torsarter, and S. Bakke, Petrophysical laboratory, *Marine and Petroleum Geology*, 1996.

Hoshen, J., Percolation analog for a two component liquid vapor system, *Chem. Phys. Lett.*, *75*, 347–349, 1980.

Hoshen, J., and R. Kopelman, Percolation and cluster distribution I. Cluster multiple labeling technique and critical concentration algorithm, *Phys. Rev. B*, *14*, 3438–3445, 1976.

Hoshen, J., P. Klymko, and R. Kopelman, Percolation and cluster distribution III. Algorithm for the site-bond problem, *J. Stat. Phys.*, *21*, 583–600, 1979.

Hui, M. H., and M. J. Blunt, Effects of wettability on three-phase flow in porous media, *J. Phys. Chem. B*, *104*, 3833–3845, 2000.

Kinney, J. H., D. L. Haupt, M. C. Nichols, T. M. Breunig, G. Marshall, and S. J. Marshall, The X-ray tomographic microscope: 3-dimensional perspectives of evolving microstructures, *Nucl. Instr. Meth. A*, *347*, 480–486, 1994.

Knackstedt, M. A., S. J. Marrink, A. P. Sheppard, W. V. Pinczewski, and M. Sahimi, Invasion percolation on correlated and elongated lattices: Implications for the interpretation of residual saturations in rock cores, *Trans. Porous Media*, *44*, 465–485, 2001.

Kovscek, A. R., H. Wong, and C. J. Radke, A pore-level scenario for the development of mixed wettability in oil reservoirs, *AlChE J.*, *39*, 1072–1085, 1993.

Lenormand, R., Pattern growth and fluid displacements through porous media, *Physica A*, *140*, 337–353, 1986.

Lenormand, R., and C. Zarcone, Role of roughness and edges during imbibition in square capillaries, *SPE 13264. Proceedings of the Ann. Tech. Conf. and Exhib. of the SPE, Houston, Texas*, 1984.

Lenormand, R., C. Zarcone, and A. Sarr, Mechanisms of displacements of one fluid by another in a network of capillary ducts, *J. Fluid. Mech.*, *16*, 3365–3376, 1983.

Li, Y., and N. Wardlaw, The influence of wettability and critical pore-throat size ratio on snap-off, *J. Colloid Interface Sci.*, *109*, 461–472, 1986.

Lin, C., and M. H. Cohen, Quantitative methods of microgeometric modelling, *J. Appl. Phys.*, *53*, 4152, 1982.

Lowery, M. I., and C. T. Miller, Pore-scale modeling of nonwetting-phase residual in porous media, *Water Resour. Res.*, *31*, 455–473, 1995.

Ma, S., G. Mason, and N. R. Morrow, Effect of contact angle on drainage and imbibition in regular polygonal tubes, *J. Colloid Interface Sci.*, *117*, 273, 1996.

Man, H. N., and X. D. Jing, Pore network modelling of electrical resistivity and capillary pressure characteristics, *Trans. Porous Media*, *41*, 263–285, 2000.

Mayer, R. P., and R. A. Stowe, Mercury-porosimetry breakthrough pressure for penetration between packed spheres, *J. Colloid Interface Sci.*, *30*, 893–911, 1965.

McDougall, S. R., and K. S. Sorbie, The impact of wettability on waterflooding: Pore-scale simulation, *SPE Reservoir Eng.*, *10*, 208–213, 1995.

Moreira, R. G., and M. A. Barrufetb, Spatial distribution of oil after deep-fat frying of tortilla chips from a stochastic model, *J. Food Engrg.*, *27*, 279–290, 1996.

Morrow, N. R., The effect of surface roughness on contact angle with special reference to petroleum recovery, *J. Can. Pet. Technol.*, *14*, 42–53, 1975.

Morrow, N. R., H. T. Lim, and J. S. Ward, Effect of crude-oil-induced wettability changes on oil recovery, *SPE Form. Eval.*, *1*, 89–95, 1986.

Øren, P. E., S. Bakke, and O. I. Arntzen, Extending predictive capabilities to network models, *Soci. Petro. Engrg. J.*, *3*, 324–336, 1998.

Patzek, T. W., Verification of a complete pore network simulator of drainage and imbibition, *Soci. Petro. Engrg. J.*, *6*, 144–156, 2001.

Patzek, T. W., and J. D. Kristensen, Shape factor and hydraulic conductance in noncircular capillaries: II. Two-phase creeping flow, *J. Colloid Interface Sci.*, *236*, 305–317, 2001.

Patzek, T. W., and D. B. Silin, Shape factor and hydraulic conductance in noncircular capillaries: I. One-phase creeping flow, *J. Colloid Interface Sci.*, *236*, 295–304, 2001.

Powers, S. E., and M. E. Tamblin, Wettability of porous media after exposure to synthetic gasolines, *J. Contam. Hydrol.*, *19*, 105–125, 1995.

Powers, S. E., W. H. Anckner, and T. F. Seacord, Wettability of NAPL-contaminated sands, *J. Environ. Eng.*, *122*, 889–896, 1996.

Reeves, P. C., and M. A. Celia, A functional relationship between capillary pressure, saturation and interfacial area as revealed by a pore-scale model, *Water Resour. Res.*, *32*, 2345–2358, 1996.

Sahimi, M., Flow phenomena in rocks: From continuum models to fractals, percolation, cellular automata, and simulating annealing, *Rev. Mod. Phys.*, *65*, 1393–1535, 1993.

Salathiel, R. A., Oil recovery by surface film drainage in mixed-wettability rocks, *J. Petrol. Technol.*, *25*, 1216–1224, 1973.

Tuller, M., D. Or, and L. M. Dudley, Adsorption and capillary condensation in porous media: Liquid retention and interfatial configurations in angular pores, *Water Resour. Res.*, *35*, 1949–1964, 1999.

Wilkinson, D., and J. F. Williamsen, Invasion percolation: A new form of percolation theory, *J. Phys. A*, *16*, 3365–3376, 1983.

Zhang, L., and N. A. Seaton, Simulation of catalyst fouling at the particle and reactor levels, *Chem. Engrg. Sci.*, *51*, 3257–3272, 1996.

Ahmed Al-Futaisi, Department of Civil and Environmental Engineering, University of California at Berkeley, CA, 94720, USA. (futaisi@uclink4.berkeley.edu)

Tad W. Patzek, Department of Civil and Environmental Engineering, University of California at Berkeley, CA, 94720, USA. (patzek@ce.berkeley.edu)

(Received _____.)